![Chalmers University of Technology logo](AVANCEZ 1829)

CHALMERS

UNIVERSITY OF TECHNOLOGY

Surface chemical and geometrical properties of pure copper powder intended for binder jetting and sintering

(article starts on next page)

RESEARCH ARTICLE

Surface chemical and geometrical properties of pure copper powder intended for binder jetting and sintering

Lars Nyborg [ORCID] | Yu Cao [ORCID]

Department of Industrial and Materials Science, Chalmers University of Technology, Gothenburg

Correspondence
Lars Nyborg, Department of Industrial and Materials Science, Chalmers University of Technology, Gothenburg, Sweden.
Email: lars.nyborg@chalmers.se

One novel important application of sinter-based additive manufacturing involving binder jetting is copper-based products. Three different variants of nominally pure copper powder having particle size distributions with D90 < 16, 22, or 31 μm were investigated in this study. The packing behavior and the flow properties using dynamic test and shear cell, as well as specific surface area were evaluated. The analyses employed illustrate the multidimensional complexity. Because different measurements capture different aspect of the powder, it is imperative to apply a characterization approach involving different methods. Surface chemical analysis by means of X-ray photoelectron spectroscopy (XPS) showed that all powder variants were covered by Cu_2O, CuO, and $Cu(OH)_2$, with Cu_2O being dominant in all cases. The finest powder with D90 < 16 μm tended to have higher relative amount of copper in divalent state. The average apparent oxide thickness estimated by XPS depth profiling showed that the two coarser variants had similar overall average oxide thickness, whereas the finest one possessed smaller oxide thickness. The surface chemistry of the powder grades is found to be related to their rheological behavior in dynamic condition. Considering the specific surface areas in combination with the average oxide thicknesses, the amount of surface bound oxygen was estimated to be about ∼220 ppm for all three variants. Specific concerns need to be taken during the sintering of powder to keep oxygen level below that of electrolytic pitch copper (400 ppm).

KEYWORDS
binder jetting, Cu powder, powder packing, rheology, surface chemistry, XPS

1 | INTRODUCTION

Binder jetting is a growing technology in metal additive manufacturing (AM). The technology comprises a printing stage in which a binder is deposited with high precision onto a powder bed in accordance with the pre-set digital model for the part in layer-wise manner. Thereafter, the printed parts are de-bound and sintered to final density. Compared with other AM technologies using laser or electron beam, binder jetting does not employ heat sources with high power. This

means less problems related to residual stresses, distortion, and shrinkage. In addition, binder jetting is more cost-effective and is able to print large and complex component without the need for support structures.

One novel important application of sinter-based additive manufacturing involving binder jetting is copper-based products. Additive manufacturing of copper-based products using other powder bed fusion methods like selective laser melting (SLM) and electron beam melting (EBM) are associated with some specific

aspects. Even if both are successfully implemented in practice today in case of pure copper,[1,2] the low laser absorptivity in the former case poses challenges that need to be circumvented and the fact that EBM requires relatively coarse powder (40–80 μm) always means inherently rougher part surfaces and the keeping of the part being built at elevated temperature makes it difficult to create, for example, narrow channels. In the recent years, binder jetting additive manufacturing of copper has been focused on the impact of powder feedstock, printing parameters, binder type, and post processing including sintering and hot isostatic pressing (HIP). Particle sizes and size distributions play an important role in the green and post-processed parts. It has been reported that bimodal powder mixtures can improve powder spreading in terms of Hausner ratio, powder bed density, and sintered density compared with the unimodal powders.[3,4] With optimized powder recoating mechanism, fine copper powder with average particle size of ∼5 μm results in improved tensile properties compared with coarser powder and bimodal powder.[5] Nanoparticles are expected to behave as a sintering aid and increase sintering. However, when adding nanoparticles to the powder,[6] a significant increase in porosity is observed in the printed parts during the curing process. Regarding sintering, hydrogen atmosphere is able to improve the purity and the sintered density of the final copper product.[7] In addition, HIP can be used as a post-process heat treatment of sintered parts to improve the final part density, tensile strength, and ductility.[8–10] Relative density of 97.3% together with promising material properties including tensile strength, thermal conductivity, and electrical conductivity[9] have been achieved by HIP of printed and sintered parts created via bimodal powder distributions.

One major disadvantage of binder jetting compared with other AM technologies using laser or electron beam is the lower density of the fabricated components. The characteristics of the powder feedstock play an important role on the interaction between binder and powder, the quality of both the green and sintered parts. As for any powder-bed additive manufacturing technology, it is perhaps even more important to understand the characteristics of the original powder to be used in a two-stage processing like binder jetting involving a sintering stage. By virtue of the fine particle size of the powder being used, typically below 20 and 30 μm, the processing route of binder jetting combines good printability and sintering ability. This, however, means powder with high specific surface area (SSA) potentially imposes challenges with respect to spreading behavior of the powder as it is laid out across the powder bed. It also constitutes a source for oxygen as every metal particle will be covered with oxide of minimum a few nanometers in thickness. For example, the native oxide on iron in air would be about 3 nm in thickness,[11] which for an iron particle of 10 μm in size covered with Fe_2O_3 would constitute a minimum oxygen level of 360 ppm attributed to surface bound oxygen. For a copper particle of similar size with a typical oxide layer thickness of 2 nm,[12] the corresponding level of surface bound oxygen would estimate at 170 ppm. Consequently, powder surface conditions are of prime importance as the surface oxide must be reduced in part or at least allow mass transfer across it to allow for sinter necks to form

and grow.[13] It is clear that any residual oxide inclusions will both affect the sintering rate and the reachable sintered density.[14] Apart from this, the shape and size distribution, which would impact on initial powder packing and hence influence on homogeneity of powder distribution when spreading a powder layer, should be considered as well. These geometrical powder characteristics will affect the success of sintering in terms of isotropic shrinkage and risk for distortion for given sintering process. So far, the binder jetting has evolved to be fully implemented in manufacturing with parts reaching near full density with consistently final closed porosity. For further development, using finer powder could be an attractive route to reach even better performance for small feature manufacturing. For this reason, a comparative study of three different variants of pure copper powder with different size distributions was employed, in which a full assessment of powder characteristics like sizes, size distribution, and SSA was coupled with rheological characterization and surface chemical analysis by means of X-ray photoelectron spectroscopy (XPS). The study has been limited to the actual powder characterization using the above-mentioned tools, but with the intention to pave the way for using finer copper powder in sinter-based additive manufacturing technologies.

2 | MATERIAL AND METHODS

Three different variants of fresh nominally pure Cu powder (99.9%) were provided by Carpenter Powder Products; one grade with D90 < 31 μm and two grades with D90 < 22 and 16 μm, respectively. The particle size distributions of the three grades are measured by laser diffraction analysis using Mastersizer 3000 manufactured by Malvern Ltd.

The flow properties of different variants of powder intended for binder jetting were evaluated using a FT4 powder Rheometer from Freeman Technology, UK in a manner reported previously.[15] Prior to measurement, the powder was conditioned under ambient conditions for 1 h. Conditioning is a mechanical process designed to loosen and slightly aerate the powder. The purpose is to remove pre-compaction and the variability introduced by the operator during sample loading. By using built-in balance and volume of the test vessel, conditioned bulk density (CBD) was measured during the dynamic test. Both the confined and unconfined dynamic flow tests were performed. Confined flow meant the blade moved downwards. The powder was forced towards the bottom of the containing vessel and thus under compressive stress. The flow energy was measured repeatedly at a specific blade tip speed of 100 mm/s for seven times with a conditioning cycle between each. Basic flowability energy (BFE) is the stabilized flow energy from Test 7, whereas the stability index (SI) is the ratio of energy in Test 1 to energy in Test 7. Subsequently, three additional tests[8–11] at reducing blade speeds were conducted. The flow rate index (FRI) is the ratio of flow energy in Test 11 to energy in Test 8. This provided information of the sensitivity to flow rate. The powder was then manually tapped 50 times followed by measurements of flow energy (CEtap50) and density (BDtap50). In unconfined dynamic

flow tests of conditioned powder, on the contrary, the blade moved upwards, and consequently, the powder was not consolidated. The energy expended in establishing the flow pattern is specific energy (SE). To determine the shear strength properties, shear cell measurements at different levels of normal stress with a pre-compaction of 6 kPa were conducted as well. The obtained shear stress and normal stress pairs were plotted to generate yield locus. Cohesion was defined as the shear stress required to deform the powder when no normal stress is applied. Major principal stress (σ_1) and unconfined yield strength (σ_c) were determined by fitting Mohr stress circles to the yield locus. Flow function is defined as the ratio of σ_1 to σ_c. The parameters of flow properties characterized using FT4 powder Rheometer in this study is summarized in Table 1. In addition, the SSA (BET) according to the BET method[16] was determined via nitrogen gas adsorption using a Gemini VII Micromeritics. Prior to measurement, the sample was degassed at 200°C in a nitrogen flow to remove moisture.

The different variants of powder were then characterized by means of XPS using a PHI VersaProbe III Scanning XPS microprobe. Powder was pressed slightly on flat pure Al plates for the analysis, and the lateral resolution of analysis was kept at 100 μm using 25 kW monochromatized AlK$_\alpha$ X-ray beam. The experimental set-up of the instrument is such that the incoming X-ray beam hits the sample target at normal incidence and that the analysis direction is at 45° compared with the sample surface. For powder sample with spherical geometry, simplified to 2D-cross-sectional view, this typically means take-off angles at between 90 and 0°. Energy calibration was obtained with reference to Cu2p$_{3/2}$, Ag3d$_{5/2}$, and Au4f$_{7/2}$ positions at 932.6, 368.2, and 84.0 eV binding energies, respectively. The compositional depth profiling was employed by mean of successive ion etchings and analyses using a 2 kV argon ion beam and ion current of 7 mA, scanned 5 × 5 mm^2, which produced an etch rate of 1.1 nm/min as calibrated on flat tantalum sample with known Ta$_2$O$_5$ overlayer thickness. The set-up of ion etching had a nominal angle of ion gun of 33° with respect to flat surface. This etch rate was assumed to be representative estimate when depth profiling the powder samples, and

hence, all depths quoted hereafter refer to thickness values on Ta$_2$O$_5$ units. In previous work, a model[17,18] has been developed and verified to account for the spherical shape of powder in XPS depth profiling. Using this model, the position of the oxide/metal interface is assigned to be where the metal intensity reaches approximately 60% of its maximum value for very thin oxide layers of concern in this study. This measure is also found to correlate with oxide thickness estimate using the half maximum intensity of the O1s peak, applied in this study.

3 | RESULTS AND DISCUSSION

3.1 | Particle size distributions

The particle size distributions in terms of cumulative weight percentage of the three grades are shown in Figure 1. It is clear that the powder variant D90 < 16 μm possessed significantly more fine powders compared with other two variants. The weight percent of powder particles smaller than 10 μm is ~59%, 38%, and 31% for D90 < 16, 22, and 31 μm, respectively.

3.2 | Rheological characterization

The flow behavior of powder plays an important role in additive manufacturing. The factors that affect the powder flowability include inherent material properties; powder size distribution and shape; processing; and environment such as storage time, humidity, and temperature. Different methods are available for characterization of flow behavior of powder.[19] Different measurements capture different aspect of the powder in various processes. Dynamic test and shear cell are two characterization methods of flowability.[15] The former one takes the actual flow (dynamic condition) into consideration and provides information of powder behavior during mixing, transfer, and filling of, for example, molds. The shear cell test is used for

TABLE 1 Flow properties characterized using FT4 powder rheometer in this study

| Parameters	Acronyms	Conditions	Notes
Conditioned bulk density	CBD	After conditioning	Conditioning was performed under ambient conditions for 1 h
Basic flowability energy	BFE	Confined dynamic test	Tests 1–7 were performed at a specific blade tip speed. BFE was the stabilized flow energy from Test 7
Stability index	SI	Confined dynamic test	Stability index ratio of flow energy in Test 1 to energy in Test 7
Flow rate index	FRI	Confined dynamic test	Tests 8–11 were performed at reducing blade tip speed. FRI was the ratio of flow energy in Test 11 to energy in Test 8
Flow energy at tapping	CEtap50	After tapping 50 times	—
Bulk density at tapping	BDtap50	After tapping 50 times	—
Specific energy	SE	Unconfined flow test	—
Cohesion	—	Shear cell	Shear stress required to deform powder when no normal stress was applied
Flow function	FF	Shear cell	Ratio of major principal stress σ_1 to unconfined yield strength σ_c
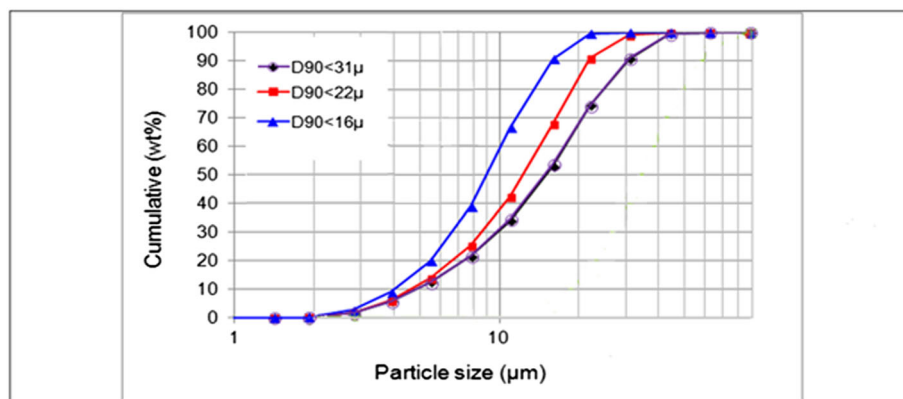
TABLE 2 Rheological characterization of variants of Cu powder studied

Powder	BFE (mJ)	SI	FRI	SE (mJ/g)	CBD (g/ml)	CEtap50 (mJ)	BDtap50 (g/ml)
D90 < 31 μm	636	1.04	1.56	3.43	5.01	3,115	6.00
D90 < 22 μm	568	1.02	1.54	3.26	4.82	3,235	5.78
D90 < 16 μm	528	1.18	1.75	4.11	4.63	3,764	5.58

Abbreviations: BDtap50, bulk density at tapping; BFE, basic flowability energy; CBD, conditioned bulk density; CEtap50, flow energy at tapping; FRI, flow rate index; SE, specific energy; SI, stability index.
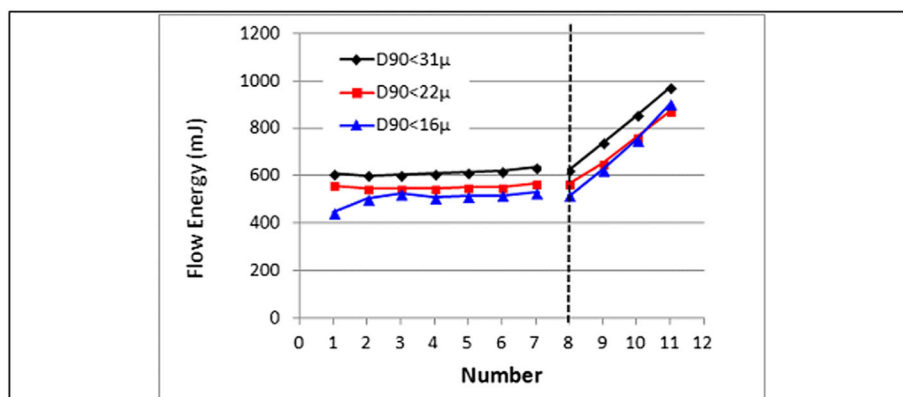
characterizing the behavior of the powder during the transition from a static state to a dynamic state, that is, flow initialization. This is the case when opening the bottom of a hopper.

When comparing the three variants of fresh powder having different size distributions, the most obvious difference regarding the packing ability is the decrease in CBD achieved as particle size distribution has smaller maximum size, see Table 2. This is also reflected by the corresponding decrease in BFE, as seen in Figure 2, owing to less material to move during compression and shearing motion of the powder while the blade is descending through the powder bed. In general, the investigated powders are relatively stable, and the sensitivity of the powder to flow rate is moderate in the confined flow condition when powder is consolidated, as demonstrated by the SI and FRI in Table 2. The coarser Cu powder variants of D90 < 31 and 22 μm variants have similar SI and FRI. For the finest powder with D90 < 16 μm, there is a slight increase of instability and sensitivity to flow rate. In addition, significant compaction at

tapping (BDtap50) and the corresponding large increase in flow energy (CEtap50) after tapping are observed for all three variants. Different from the variation of BFE, flow energy after tapping increases with the decrease of D90.

The SE, measured at moving the blade upwards is the resistance of the powder to flow when close to a non-consolidated or stress-free state. It is characteristic of an unconfined flow and gives an indication of the degree of powder cohesivity. Actually, the Cu < 16 μm variant appears to be more cohesive than two coarser variants. Often, cohesive powder is more sensitive to changes in flow rate. This is consistent with the increased FRI of this powder variant. In summary, the powder size and its distribution affect the powder flowability significantly in a dynamic test in current study, especially for the finest powder grade.

Figure 3 shows the shear stresses required to move the shear cell at various normal stress levels. Table 3 presents the output of the shear cell measurements as derived from yield locus of the powder
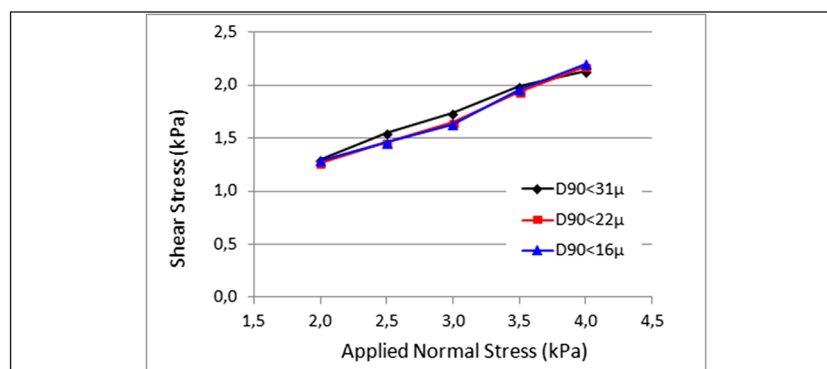
TABLE 3   Results from shear testing and specific surface areas determined by the BET method

Material and batch	Cohesion (kPa)	FF	BD (g/ml)	SSA (m²/g)
D90 < 31 μm	0.48	6.2	5.07	0.073
D90 < 22 μm	0.32	8.8	4.98	0.079
D90 < 16 μm	0.33	8.6	4.83	0.113

Abbreviations: BD, bulk density; FF, flow function; SSA, specific surface area.

variants in Figure 3 including results from the BET measurements in terms of SSA. Cohesion is the shear stress required to deform the powder when no normal stress is applied. As can be seen from Table 3, powder with D90 < 31 μm has the highest cohesion, whereas the values are almost equivalent for two fine variants. The flowability qualitatively estimated from FF gives the similar trend. It seems that shear test is less sensitive to the increase of the fines content compared with dynamic test. There might be a threshold below which the powder behavior changes little in a shear test. Nevertheless, powder with D90 < 31 μm has worse flow properties than the others in a shear test. It should be noted that the SSA clearly deviates between the two finer particle size variants, whereas the difference in SSA between D90 < 31 and 22 μm variants is instead smaller than expected, possibly because of more fines, not depicted by particle size distribution measurements (c.f. Figure 1). This supposedly compensates for the overall particle size distributions. Nevertheless, the results in Table 3 indicate that the fine powder with large SSA possessed better flow properties in a shear test, which characterized the behavior of the powder during the transition from a static state to a dynamic state, that is, flow initialization.

Powder flow behavior may change significantly during different stage of processing. This is confirmed by the flowability data of the finest powder variant D90 < 16 μm in Tables 2 and 3. As stated previously, dynamic test concerns actual flow (dynamic condition, Table 2), whereas shear cell provides information during the transition from a static state to a dynamic state (Table 3). Despite of good flow performance in flow initialization (cohesion and FF) and low BFE in dynamic test, the finest powder variant D90 < 16 μm has an increase in SE, instability (SI), and sensitivity to flow rate (FRI). Especially, there is large increase in tap density BDtap50 and flow energy CEtap50 after tapping. This fact can potentially cause problems at exposure when shaking or vibrating powder. Nevertheless, the powder grades tested

in this study are supposed to contain certain fraction of fines, which would add challenges for the powder handling. When considering all rheometer data, it seems that the D90 < 22 μm shows the better overall flow performance among the three variants. Still, the significant impact of tapping may cause processing problems in binder jetting.

3.3 | Surface chemical analysis

Because the surface chemical condition constitutes an additional factor that may affect particle–particle interaction and hence flow as well as the sintering, it is of paramount importance to couple this information as well to the overall powder characterization. Considering oxides of copper, CuO is a weak base, whereas Cu_2O is supposed to show stronger basic properties in a Lewis sense.[20] Both are characterized as being metal deficient p-type extrinsic semiconductors, with band gaps of 1.2 and 2.17 eV for CuO and Cu_2O, respectively. In as-received conditions, it can be expected that there is hydroxide formation as well. Let us now address the surface chemistry of the three variants of copper powder included in this study.

The XPS high-energy resolution spectra of $Cu2p_{3/2}$ region including shake-up satellite were recorded from the surface of three powder variants, as shown in Figure 4A. For three powder variants, the main Cu $2p_{3/2}$ peak is located at 932.5 eV, indicating the presence of Cu_2O and/or metallic Cu. The shake-up structure on the higher binding energy side provided evidence of Cu^{2+}, as marked by solid arrow in Figure 4A. To distinguish properly between Cu_2O and Cu, Auger Cu $L_3M_{45}M_{45}$ peak was also recorded, as exhibited in Figure 4B. For three powder variants, the main component of Cu $L_3M_{45}M_{45}$ Auger peak is located at apparent binding energy position of 569.9 eV, corresponding to approximate $L_3M_{45}M_{45}$ kinetic energy of 916.7 eV,
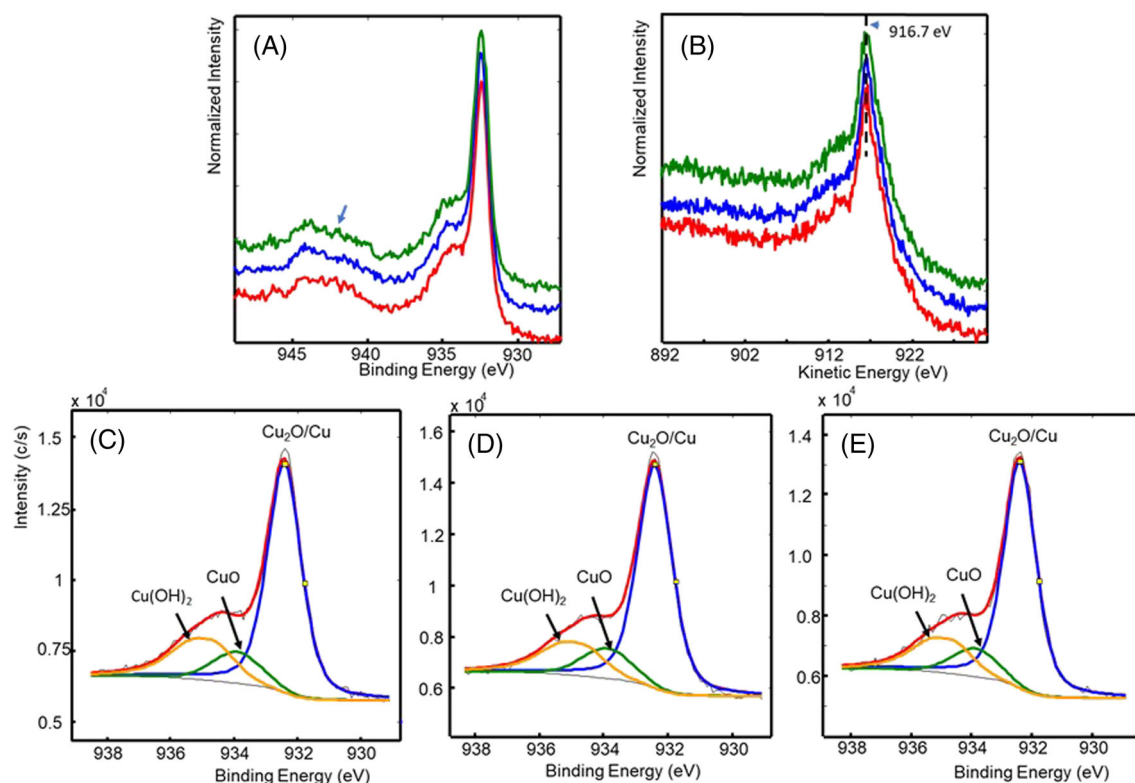
FIGURE 4 X-ray photoelectron spectroscopy (XPS) high-energy resolution spectrum of (A) $Cu2p_{3/2}$ core level and (B) Cu $L_3M_{45}M_{45}$ Auger peak recorded from the surface of copper powders. Curve fitting of $Cu2p_{3/2}$ core level is also shown for powders with distribution of particle sizes (C) D90 < 16, (D) 22, and (E) 31 μm

TABLE 4 XPS binding energy positions of $Cu2p_{3/2}$ and O1s core level peaks for copper compounds, data from Lodes et al[2]

Compound	Cu2p3/2 (eV)	O1s (eV)
Cu_2O	932.5	530.7
CuO	933.9	529.7
$Cu(OH)_2$	934.8	531.8

TABLE 5 Relative amounts (mole%) of Cu species on surfaces of different Cu powder variants

Powder	Cu_2O^a	CuO	$Cu(OH)_2$
D90 < 16 μm	69	11.5	19.5
D90 < 22 μm	71.5	12	16.5
D90 < 31 μm	72	11	17

[a]Possibly including small contributions from Cu owing to X-ray photoelectron spectroscopy (XPS) peak overlap.

whereas the peak representing Cu_2O/Cu was recorded at 932.5 eV. This correlation is strongly indicative for Cu_2O rather than Cu.[12] The difficulty to observe metallic Cu at kinetic energy of ∼918.4 eV in Auger Cu $L_3M_{45}M_{45}$ peak confirmed this again. Consequently, the overall picture, as depicted from the data in Table 5 and the consistency in analysis and its evaluation, is that all powder variants have Cu_2O as main surface products together with divalent copper compounds either in oxide or hydroxide. For pure Cu, combination of Cu_2O and CuO is expected from thermodynamics modeling,[21] and oxygen activity required for formation of CuO is lower than for less pure copper like phosphorus-deoxidized copper. Presumably, the presence of hydroxide only reflects transition of the CuO into $Cu(OH)_2$ on the outermost surface.

To depict the surface chemistry, a procedure developed previously for copper powder has been used.[12] From that work, the peak positions of $Cu2p_{3/2}$ and O1s XPS signals for Cu_2O, CuO, and Cu $(OH)_2$ were experimentally derived in accordance with prior literature

values. Table 4 summarizes the results. With this input as basis, curve fitting of the core level $Cu2p_{3/2}$ line was performed for the three variants of copper powder using asymmetric Gauss-Lorentz function by means of Multipak software, as presented in Table 5 and Figure 4C–E. Notice fixed fitting parameters were applied in all cases including peak positions, peak widths, Gaussian ratio of individual peak, peak tail length, and peak tail scaling. As can be seen, there is good overall fit using the three peaks assigned to Cu_2O, CuO, and Cu $(OH)_2$ in accordance with Table 4. The goodness of fit is also indicated by the small chi-square values that are similar for three powder variants. The relative amounts of different chemical species can be obtained by considering the area of each fitted peak assuming same sensitivity factors for the compounds. The overall surface composition is within scope and range of the analysis is similar for all powder variants. Would there be any difference, it is then that the finest powder
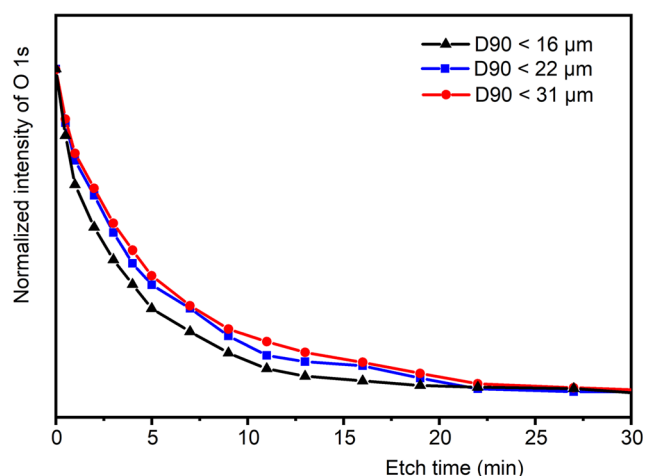
FIGURE 5 X-ray photoelectron spectroscopy (XPS) depth profiles showing O1s peak intensity versus etch time used for determining the apparent average oxide thickness for the powder variants studied. The nominal ion etch rate applied was 1.1 nm/min as calibrated on Ta_2O_5

TABLE 6 Apparent average oxide thicknesses derived from X-ray photoelectron spectroscopy (XPS) depth profiles in Figure 5

Sample	Oxide thickness (nm)
D90 < 16 μm	2.2
D90 < 22 μm	3.3
D90 < 31 μm	3.5

(D90 < 16 μm) tends to have a higher share of Cu^{2+} in the surface perhaps in the form of $Cu(OH)_2$.

Besides the surface composition, the overall oxide thickness is of importance when considering surface bound oxygen for the different variants of copper powder. This oxide thickness can be estimated by XPS depth profiling as outlined in previous work for Cu powder intended for laser powder bed fusion.[12] Figure 5 below shows the XPS depth profiles in terms of oxygen intensity versus etch time obtained by means of successive ion etchings and analyses. The nominal etch rate applied was 1.1 nm/min as calibrated on flat tantalum sample with known Ta_2O_5 overlayer thickness. Taking the measure $(I_O^{max} - I_O^{min})/2$ as an indicator for the oxide/metal interface, the apparent average oxide thicknesses derived for the different powder variants are shown in Table 6.

From the oxide thickness data presented in Table 6, it can be seen that the two coarser powder variants have basically the same overall oxide thickness, whereas the finer powder tends to show slightly thinner oxide. Considering that all variants represent gas-atomized powder, these observations are not unexpected based on the following arguments. As shown by Nyborg and Olefjord[22] and Grinder and Ericsson[23] for gas-atomized metal powder, the average oxide thickness is basically the same for a wide particle size range, whereby the amount of surface bound oxygen scales with the SSA or simply the inverse of the particle size. However, when applying surface chemical

analysis in more detail on different size fractions of gas-atomized 12% Cr-steel powder from the same batch, it was demonstrated by Nyborg and Norell[24] that the finest powder grade with size below about 20 μm had smaller oxide thickness than the rest of the powder. The availability and transfer of oxygen from the atomizing gas is supposed to be the rate controlling factor for the potential oxidation during atomization considering the low availability of oxygen gas (ppm levels).[22] This fact means that mass and heat transfer balance one another for most particle sizes, expect for the really small ones. Hence, the less oxidation tendency for the powder with D90 < 16 μm is suggested to be a consequence of this aspect as this powder has high share of fines as evidenced from the particle size distribution measurements (see Figure 1). Obviously, such finer powder is not more reactive when handled in air after atomization. Would uncontrolled oxide growth be case, greater oxide thickness should have been observed. Instead, it seems like there is somewhat higher amount of divalent Cu, that is, $Cu(OH)_2$ for the D90 < 16 μm variant in the surface. The powders have been stored in same manner in desiccator prior to XPS analyses, but it cannot be disregarded that there could be size effect with respect to storage if the surface hydroxide content is indicative for a consistent difference. As a matter of fact, when copper oxide is exposed to humid conditions, it will degrade as shown by Tamai,[25] namely, with increasing humidity, there is a decrease in oxide thickness, whereas the decrease in humidity increases the oxide thickness. The humidity in this sense affects also contact resistance in both static and sliding contacts. With this effect in mind and now the surface compositions of the powder grades are coupled with their rheological behavior. The powder with D90 < 16 μm has higher share of Cu^{2+} in the surface (Table 5). This is consistent with the increase of CEtap50, SE, SI, and FRI in dynamic test, compared with other two coarser powder grades that have similar oxide thickness and surface composition. Interestingly, these two coarser powder grades have comparable CEtap50, SE, SI, and FRI. The lower BFE for fine powder is simply because of the lower bulk density, leading to less material to move during compression and shearing motion of the powder while the blade is descending through the powder bed. For the shear test, it should be pointed out that the two finer variants (<16 and <22 μm) were much closer to one another in terms of cohesion and flow function than what could be anticipated for their particle size distribution (c.f. Figure 1). Thus, it is suggested that the difference in surface composition for the finer powder compared with the two other grades provides a counterbalancing factor.

Even if the actual investigation of the sintering behavior of the studied powder variants is outside the scope of the present study, a few remarks can here be made. First, the overall surface bound oxygen $X_{O,S}$ can be depicted by applying the equation $X_{O,S} = SSA \cdot t_{OX} \cdot X_{O,OX} \cdot \rho_{OX}$, where SSA is specific surface area (cm²/g), $X_{O,OX}$ is the mass fraction of oxygen in the oxide, t is the thickness of oxide (cm), and ρ_{OX} is the oxide density (g/cm³). For simplicity, let us assume same XPS sensitivity factors for different Cu chemical species, the area ratio from curve fitting of $Cu2p_{3/2}$ line gives the mass fraction of Cu involved in the different compound. By knowing the density and oxygen fraction, the thickness of each Cu oxide species can be

TABLE 7 Parameters used for calculation of oxygen levels related to surface bound oxygen

Oxide species	Density ρ_{OX} (g/cm^3)	Mass fraction of oxygen $X_{O,OX}$	Thickness t_{ox} of different oxide species in three powder variants (nm)		
			D90 < 16 μm	D90 < 22 μm	D90 < 31 μm
Cu_2O[a]	6.00	0.11	1.32	2.10	2.24
CuO	6.31	0.20	0.21	0.34	0.33
$Cu(OH)_2$	3.37	0.33	0.67	0.86	0.94
Specific surface area (SSA, m^2/g)			0.113	0.079	0.073
Oxygen levels related to surface bound oxygen (ppm)			213	219	214

[a]Dominant oxide species.

obtained as shown in Table 7. With the SSA values for the different powder grades (Table 3), the oxygen levels related to surface bound oxygen can be estimated by applying the rule of mixture and the equation mentioned previously. The obtained oxygen levels are 213, 219, and 214 ppm (Table 7) for the D90 < 16, 22, and 31 μm variants, respectively. The closeness of the figures is related to combination of oxide thickness and SSA for the different grades. Notice the apparent average oxide thickness is calculated based on the etch rate of Ta_2O_5 with known overlayer thickness. Considering the larger argon sputtering yield of Cu compared with Ta during depth profiling, the overall oxide thickness and consequently the oxygen levels related to surface bound oxygen might be underestimated. On the other hand, the critical level is about 400 ppm for pure copper, electrolytic tough pitch (ETP) grade. At above 400°C, the reaction $Cu_2O + H_2 = Cu + H_2O$ becomes viable whereby water vapor induced blistering and associated embrittlement become risks. In the case of binder jetting, after printing stage, it is of course crucial to reduce the copper oxide on the powder surface in an early stage during sintering. The oxygen levels indicated that this is an important concern for appropriate sintering. Using hydrogen as effective reduction agent then implies that the oxygen level must be significantly reduced before reaching the target sintering temperature. For the particle size distributions of concern here, final target temperatures can be up to below the melting temperature of copper.[9] This requires dedicated sintering process design to mitigate blistering effect. Furthermore, as outlined in Section 1, any residual oxide layer represents a potential restriction for sinter neck development as pointed out by Munir.[13] As modeled and shown by Ashby et al,[14] any residual oxide inclusions limit both the final reachable sintering density in solid state sintering as well as the sintering rate. Even if reduction of CuO and Cu_2O is thermodynamically viable at low temperatures, the overall control must be addressed with care.

With decreasing particle size, higher sintering activity is expected owing to higher SSA. In this respect, the fine D90 < 16 μm powder is of interest for further studies considering its comparably smaller oxide thickness. A potential drawback could be higher sensitivity to contamination during handling owing to the higher SSA and some potentially worse rheological properties, even though not being fully evident from the present study. The powder surface chemistry is also considered to be important for the surface interaction in any forming process including binder jetting. Both Cu_2O and CuO are supposed to be

basic oxides according to Lewis's acid–base concept. An important consequence is that acidic compounds like stearic acid and oleanic acid, would adsorb on the surfaces of all powder variants studied, whereas a basic compound like aniline would tend not to do so. This has for example been shown for the surface interaction with 316-L stainless powder used in metal injection molding.[26]

4 | CONCLUSIONS

Three different variants of nominally pure copper powder of interest for sinter-based additive technologies like binder jetting were characterized by means of assessing different characteristics of importance for powder packing and rheology in combination with surface chemical analysis using XPS. For these variants having particle size distributions with D90 < 16, 22, or 31 μm, the analyses employed illustrate the multidimensional complexity in judging the appropriateness of powder for optimum behavior for the intended processing route. Still, a number of important conclusions can be stated as follows.

1. With smaller average particle size, both the CBD and the tap density of the powders decreased. The BFE is related to bulk density. Finer powder with lower bulk density has reduced BFE. In all cases, there was significant impact of the tapping depicting a challenge for use in binder jetting.
2. The finest powder variant D90 < 16 μm has good flow performance in flow initialization in terms of cohesion and FF; however, it behaves less satisfied in dynamic test. When considering all rheometer data, it seems that the D90 < 22 μm showed the better overall flow performance among the three variants.
3. Having access to only particle size distribution is not enough for judging the powder behavior. Neither is the rheological characterization as such without additional information on SSA. The reason for this is supposed to be that the different measurements capture different aspect of the powder in varied process and that the role of fines at tail of size distribution is a key factor that requires multi-characterization approach to evaluate.
4. The application of surface chemical analysis (XPS) adds important information in this context. All variants of powder are shown to be covered by Cu_2O, CuO, and $Cu(OH)_2$ in line with what can be expected for pure copper. The molar amount of Cu_2O is shown to

be dominant in all three cases, but with tendency for higher relative amount of copper in divalent state (CuO and $Cu(OH)_2$) for the finest powder with D90 < 16 μm.

5. The surface chemistry of the powder grades is found to be related to their rheological behavior in dynamic condition. Higher share of Cu^{2+} in the surface of powder with D90 < 16 μm corresponds to the increase of SE, CEtap50, SI, and FRI, compared with other two coarser powder grades that have similar oxide thickness and surface composition and consequently comparable SE, CEtap50, SI, and FRI.

6. Considering that both Cu_2O and CuO are supposed to be basic oxides as well as being p-type extrinsic semiconductors, this sets the conditions for the surface interactions in the binder jetting process.

7. The XPS depth profiling revealed that the average nominal oxide thickness was 2.2, 3.3, and 3.5 nm for the powder with D90 < 16, 22, and 31 μm, showing that the two coarser variants had similar overall average oxide thickness, while the finest one showed the smallest oxide thickness.

8. Considering the SSAs in combination with the average oxide thicknesses the amount of surface bound oxygen was estimated to be about ∼ 220 ppm for all three variants.

9. The level of oxygen is such that specific concerns need to be taken during the sintering of powder to reassure proper sintering and mitigation of effects like hydrogen blistering.

ACKNOWLEDGMENTS

DATA AVAILABILITY STATEMENT

Data openly available in a public repository that issues datasets with DOIs

ORCID

Lars Nyborg https://orcid.org/0000-0002-1726-5529
Yu Cao https://orcid.org/0000-0002-1965-5854

REFERENCES

1. Colopi M, Caprio L, Demir AG, Previtali B. Selective laser melting of pure Cu with a 1 kW single mode fiber laser. *Procedia CIRP*. 2018;74: 59-63. doi:10.1016/j.procir.2018.08.030

2. Lodes MA, Guschlbauer R, Körner C. Process development for the manufacture of 99.94% pure copper via selective electron beam melting. *Mater Lett*. 2015;143:298-301. doi:10.1016/j.matlet.2014.12.105

3. Bai Y., Wagner G., Williams C.B.. Effect of bimodal powder mixture on powder packing density and sintered density in binder jetting of metals. Paper presented at: Annual International Solid Freeform Fabrication Symposium; 2015.

4. Bai Y, Wagner G, Williams CB. Effect of particle size distribution on powder packing and sintering in binder jetting additive manufacturing of metals. *J Manuf Sci Eng*. 2017;139(8):081019-081011. doi:10.1115/1.4036640

5. Miyanaji H, Rahman KM, Da M, Williams CB. Effect of fine powder particles on quality of binder jetting parts. *Addit Manuf*. 2020;36: 101587. doi:10.1016/j.addma.2020.101587

6. Bailey A.C., Merriman A., Elliott A. and Basti M.M.. Preliminary testing of nanoparticle effectiveness in binder jetting applications. Paper presented at: 27th Annual International Solid Freeform Fabrication Symposium; August 2016; Austin.

7. Bai Y, Williams CB. An exploration of binder jetting of copper. *Rapid Prototyp J*. 2015;21(2):177-185. doi:10.1108/RPJ-12-2014-0180

8. Kumara A, Baia Y, Eklundb A, Williams CB. Effects of hot isostatic pressing on copper parts fabricated via binder jetting. *Procedia Manuf*. 2017;10:935-944. doi:10.1016/j.promfg.2017.07.084

9. Kumara AY, Wang J, YB, Huxtable ST, Williams CB. Impacts of process-induced porosity on material properties of copper made by binder jetting additive manufacturing. *Mater Des*. 2019;182:10800. doi:10.1016/j.matdes.2019.108001

10. Kumara AY, Baia Y, Eklundb A, Williams CB. The effects of hot isostatic pressing on parts fabricated by binder jetting additive manufacturing. *Addit Manuf*. 2018;24:115-124. doi:10.1016/j.addma.2018.09.021

11. Nyborg L, Olefjord I. Surface analysis of REP-atomized martensitic steel powder. *Powder Metall Int*. 1988;20(2):11-16.

12. Bojestig E, Cao Y, Nyborg L. Surface chemical analysis of copper powder used in additive manufacturing. *Surf Interface Anal*. 2020;52(12): 1104-1110. doi:10.1002/sia.6833

13. Munir ZA. Surface oxides and sintering of metals. *Powder Metall*. 1981;4(4):177-180. doi:10.1179/pom.1981.24.4.177

14. Ashby MF, Bahk S, Bevk J, Turnbull D. The influence of a dispersion of particles on the sintering of metal powders and wires. *Prog Mater Sci*. 1980;25(1):1-34. doi:10.1016/0079-6425(80)90013-4

15. Freeman R. Measuring the flow properties of consolidated, conditioned and aerated powders—a comparative study using a powder rheometer and a rotational shear cell. *Powder Technol*. 2007; 174(1–2):25-33. doi:10.1016/j.powtec.2006.10.016

16. Dollimore D, Spooner P, Turner A. The BET method of analysis of gas adsorption data and its relevance to the calculation of surface areas. *Surface Technol*. 1976;4(2):121-160. doi:10.1016/0376-4583(76)90024-8

17. Nyborg L, Nylund A, Olefjord I. Thickness determination of oxide layers on spherically-shaped metal powder by ESCA. *Surf Interface Anal*. 1988;12(2):110-114. doi:10.1002/sia.740120209

18. Oikonomou C, Nikas D, Hryha E, Nyborg L. Evaluation of the thickness and roughness of homogeneous surface layers on spherical and irregular powder particles. *Surf Interface Anal*. 2014;46(10–11): 1028-1032. doi:10.1002/sia.5439

19. Cain SR, Matienzo LJ. Acid-base properties of copper oxides and fluorides by means of band calculations: relevance to metal-polymer adhesion. *J Adhes Sci Technol*. 1988;2(1):395-404. doi:10.1163/156856188X00390

20. Baesso I, Karl D, Spitzer A, Gurlo A, Günster J, Zocca A. Characterization of powder flow behavior for additive manufacturing. *Addit Manuf*. 2021;47:102250. doi:10.1016/j.addma.2021.102250

21. Magnusson H., Lindberg H., Frisk K.. Validating the thermodynamic description of copper oxides and phosphates. 2015. Accessed May 3, 2021. https://skb.se/publikation/2485262/R-15-06.pdf

22. Nyborg L, Olefjord I. Surface analysis of PM martensitic stainless steel before and after consolidation: part 1: surface analysis of powder. *Powder Metall*. 1988;31(1):33-39. doi:10.1179/pom.1988.31.1.33

23. Grinder O, Ericsson U. Low temperature oxidation of inert-gas atomized steel powder. *Powder Metall*. 1985;16:295-327.

24. Nyborg L, Norell M, Olefjord I. Surface studies of powder metallurgical stainless steel. *Surf Interface Anal*. 1992;19(1–12):607-612. doi:10.1002/sia.7401901113

25. Tamai T. Effect of humidity on growth of oxide film on surface of copper contacts. *IEEE Trans Ind Electron*. 2007;E90C(7):1391-1297. doi:10.1093/ietele/e90-c.7.1391

26. Johansson E, Nyborg L. XPS study of surface-active organic compounds on fine ferrous powder. *Surf Interface Anal*. 2000;30(1):333-336. doi:10.1002/1096-9918(200008)30:13.0.CO;2-H